Neural, Parallel, and Scientific Computations 18 (2010) 33 - 46

A COMPUTATIONAL ANALYSIS TO ASSESS THE INFLUENCE OF SPECIMEN GEOMETRY ON CLEAVAGE FRACTURE TOUGHNESS OF METALLIC MATERIALS

SUNIL PRAKASH, XIAOSHENG GAO and **T. S. SRIVATSAN**
Department of Mechanical Engineering
The University of Akron, Akron, Ohio 44325-3903, USA
E-Mail (contact): xgao@uakron.edu

Abstract: The fracture response of mild steel in the domain of brittle behavior, i.e., the cleavage range, has been carefully evaluated using a weakest link statistical model, assuming the existence of a distribution of cracked carbide particles in the microstructures. Experiments have provided an evidence of both scatter in test results and the existence of constraints. Statistical-based model to include micromechanics were developed in an attempt to study and analyze the problem. The Weibull stress micro-mechanical model was used in this study to quantify the constraint effects. This was done numerically using a constraint function ($g(M)$) derived from the Weibull stress model. The non-dimensional function ($g(M)$) describes the evolution of the effects of constraint loss on fracture toughness relative to the reference condition, i.e., plane-strain, small scale yielding (SSY) (T-stress = 0). Single-edge SE(B) notched bending specimens having different crack lengths, different cross-sections and side-grooves were modeled and the constraint function ($g(M)$) was calculated. In this paper, we compare the loss in constraint for both the deep notch and shallow notch specimens for a given cross-section of the single-edge notched bend specimen (SE(B)).

Keywords: cleavage fracture, Weibull stress, toughness scaling, constraint function, finite element analysis

1. INTRODUCTION

The occurrence of transgranular cleavage in ferritic steels takes place with localized microplastic deformation when tested in the ductile-to-brittle transition (DBT) range (Wallin, 1984; Sorem, 1991). The plastic region immediately ahead of the crack front interacts with nearby traction free boundaries and breaks down the single parameter characterization of crack front stresses in terms of the J-integral (Rice, 1968). The crack-tip plastic zone in the single edge notched bend specimen (SE(B)) having a shallow crack combines well with the global bending plasticity very early during loading. A substantial loss of the crack-tip constraint follows and this essentially requires large J-values to generate sufficient stresses that are conducive for favoring the onset of failure by cleavage.

Received February 11, 2010 1061-5369 $15.00 © Dynamic Publishers, Inc

The weakest link mechanism and the deformation limit of the form $M = b\sigma_0/J_c > M_{limit}$, where b represents the ligament length, σ_0 is the yield stress of the material and J_c is the cleavage fracture toughness, have been discussed in detail in our previous paper (Prakash, 2009). Testing standards for the measurement of cleavage fracture toughness in the DBT range (ASTM E1921, 1998) requires a prudent selection of: (i) specimen type, (ii) specimen size, and (iii) nature of loading mode. This is essential for ensuring that plane strain, small-scale yielding (SSY) conditions prevail along the crack front at the time of fracture.

In this paper, we focus on comparing the effects of crack length on constraint loss ($g(M)$). We study the nonlinear response of a series of SE(B) specimens having (i) a crack length to specimen width ratio (a/W) of 0.1 and 0.5; (ii) specimen width to thickness ratio (W/B) of 1 and 2, and (iii) both with or without side grooves (20% side-grooves: 10% each side). For each of these cases we compute the constraint function $g(M)$. In our previous paper (Prakash, 2009), we considered three sets of material flow properties. In this paper, we consider only the intermediate properties ($E/\sigma_0 = 500$) with $n = 10$; where n represents the strain hardening exponent and E is the Young's modulus of the chosen metallic material. The effects of scatter in local toughness values were carefully incorporated into the analysis by varying the Weibull modulus for $m = 8$, 12, 16 and 20. Further, we attempt to introduce the applied load with the aid of rollers, which are in continuous contact with the specimen so as to capture the anticlastic bending effect. The results convincingly demonstrate the specific role of constraint effect on cleavage fracture toughness.

2. WEIBULL STRESS MODEL

The Beremin or Weibull stress model (Beremin, 1983; Mudry, 1987; Minami, 1992) provides a practical approach to quantify the evolution of crack-front effects and decay of the small-scale yielding (SSY) condition as the load is increased. The probability of cleavage fracture can be expressed as:

$$P_f(\sigma_w) = 1 - \exp\left[-\frac{1}{V_0}\int_{\bar{V}}\left(\frac{\sigma_1}{\sigma_u}\right)^m dV\right] = 1 - \exp\left[-\left(\frac{\sigma_w}{\sigma_u}\right)^m\right] \quad (1)$$

where the Weibull stress (σ_w) is given by,

$$\sigma_w = \left[\frac{1}{V_0}\int_{\bar{V}}\sigma_1^m\, dV\right]^{1/m} \quad (2)$$

The Weibull modulus (m) quantifies the degree of scatter. The scale parameter (σ_u) denotes the Weibull stress value for a cumulative probability of fracture equal to 63%. The Weibull stress is computed by integrating the maximum principal stress (σ_1) over the fracture process zone.

For the simple case of plane-strain, small-scale yielding (SSY) condition, the net volume of the cleavage process zone scales well with the thickness [$(B)\times J^2$]. The relationship between σ_w and J leads to a simpler form (Gao et. al., 1998)

$$\sigma_w^m = \varsigma B J^2 \tag{3}$$

In this equation ς is a constant that depends on the following: (i) the material flow properties (E/σ_0, υ, and n), and (ii) the Weibull model parameters (m and V_0). The thickness of the test specimen is denoted as B. For the case of three-dimensional fracture specimens, the stress and deformation fields vary over the thickness, with stronger variations favored to occur as the thickness of the test specimen diminishes relative to the in-plane dimensions. Generally, the mid-plane stresses have the largest values with sharp reductions at the traction-free outside surfaces (Prakash, 2009). Thus, the net contribution to Weibull stress (σ_w) can vary significantly over the thickness of the structure. Consequently, a simpler form of Equation (3) no longer applies.

Gao and Dodds (2000) introduced a non-dimensional constraint function [$g(M)$], to characterize the amount of constraint loss once small scale yielding (SSY) conditions breaks down in specimens under the direct influence of increased plastic deformation. The non-dimensional function $g(M)$ function is proportional to σ_w^m

$$\sigma_w^m = \varsigma B J^2 \, g(M) \tag{4}$$

In this expression $M = b\sigma_0 / J_{avg}$ and J_{avg} denotes an average value for a through-thickness J, and b is the length of the remaining ligament. The constraint function ($g(M)$) equals to 1.0 for all materials under plane-strain, SSY conditions with $T = 0$. For a three-dimensional configuration, a fracture driving force curve, that is, variation of σ_w versus J_{avg} can be generated if the $g(M)$ function has been determined. The constant ς can be calculated from plane-strain, small-scale yielding (SSY) analysis for both a given material and a given value of m. The value of the g-function can be easily solved using equation (4). For more details on the g-function please refer to our previous paper (Prakash, 2009).

3. THE NUMERICAL MODEL

3.1 Finite element model

Non-linear finite element analyses were performed using MSC/Patran (2005) for meshing, loading, and ABAQUS/Standard (2007) for solving. Here, we study the two configurations: (i) deep-notch of the single edge notch bend specimen, and (ii) shallow-notch of the single-edge notch bend specimen (SE(B)). Specific details of the finite element model are discussed in our previous paper (Prakash, 2009).

3.2 Constitutive model

The material model employed in the parametric studies follows a J_2 flow theory for conventional Mises plasticity. The finite element computations were performed

within the framework of finite-strain and an updated Lagrangian formulation. The uniaxial true stress-logarithmic strain curve obeys a simple power-law hardening model preceded by a purely linear response prior to plastic flow,

$$\frac{\varepsilon}{\varepsilon_0} = \frac{\overline{\sigma}}{\sigma_0} \quad for \quad \varepsilon \le \varepsilon_0 ; \qquad \frac{\varepsilon}{\varepsilon_0} = \left(\frac{\overline{\sigma}}{\sigma_0} \right)^n \quad for \quad \varepsilon > \varepsilon_0 \tag{5}$$

In this expression σ_0 is the yield stress, ε_0 is the yield strain, and n is the strain hardening exponent. A user defined subroutine (UHARD) was used to implement this material model into ABAQUS. The computational results are presented for a material that moderately hardens (E/σ_0 = 500 and n = 10), characteristic of many pressure vessel and pipelines steels. The Poisson's ratio (υ) was taken to be equal to 0.3.

3.3 Three-Dimensional (3-D) Finite Element Model for the SE(B) specimen

Figure 1 and 2 shows the finite element models used in the analysis. A series of geometries are chosen and modeled for:

(i) Plane-sided SE(B) specimens with a/W = 0.1 and a/W = 0.5, W/B = 1 and W/B = 2.

(ii) Side-grooved (10% on each side) SE(B) specimens with a/W = 0.1 and a/W = 0.5, W/B = 1 and W/B = 2.

Here a represents the crack length, W represents the specimen width and B represents the specimen thickness. A mesh configuration having 30 – 50 focused rings of elements in the radial direction surrounds the crack front (see Figure 1 and Figure 2). The crack tip has an initially small radius (see Figure 3) to facilitate enhancing convergence of the finite-strain solutions. The analysis makes use of finite element models having three different root radii of (i) 1.2 μm, (ii) 2.5 μm, and (iii) 5 μm. Precise details on the effect of initial radius and the reason for using different initial radius are detailed in our earlier paper (Prakash, 2009).

Displacement constraints are applied on the rigid rollers and all contacts (see Figure 1) are taken to be frictionless. The reference node on each of the roller has a prescribed displacement. Transverse displacement is given to the loading roller and all other directions are set to zero and for the support roller all the directions are set to zero.

3.4 The Small Scale Yielding model (SSY)

The plane-strain, boundary layer model (Larrson, 1973; Rice, 1974) simplifies the generation of numerical solutions for stationary cracks under conditions of small-scale yielding (SSY). With the plastic region limited to a small fraction of the domain radius (R) included in the model ($R_p < R/20$), the general form of the asymptotic crack-tip stress fields in a region well outside of the plastic region is given by (Williams, 1957)

$$\sigma_{ij} = \frac{K}{\sqrt{2\pi r}} f_{ij}(\theta) + T\,\delta_{1i}\,\delta_{1j} \tag{6}$$

In this expression K is the stress intensity factor, $f_{ij}(\theta)$ defines the angular variations of in-plane stress components, and the non-singular term T represents a tension (or compression) stress parallel to plane of the crack. Numerical solutions for $T = 0$ are generated by imposing displacements of the elastic, Mode I singular field on the outer circular boundary ($r = R$) that encloses the crack

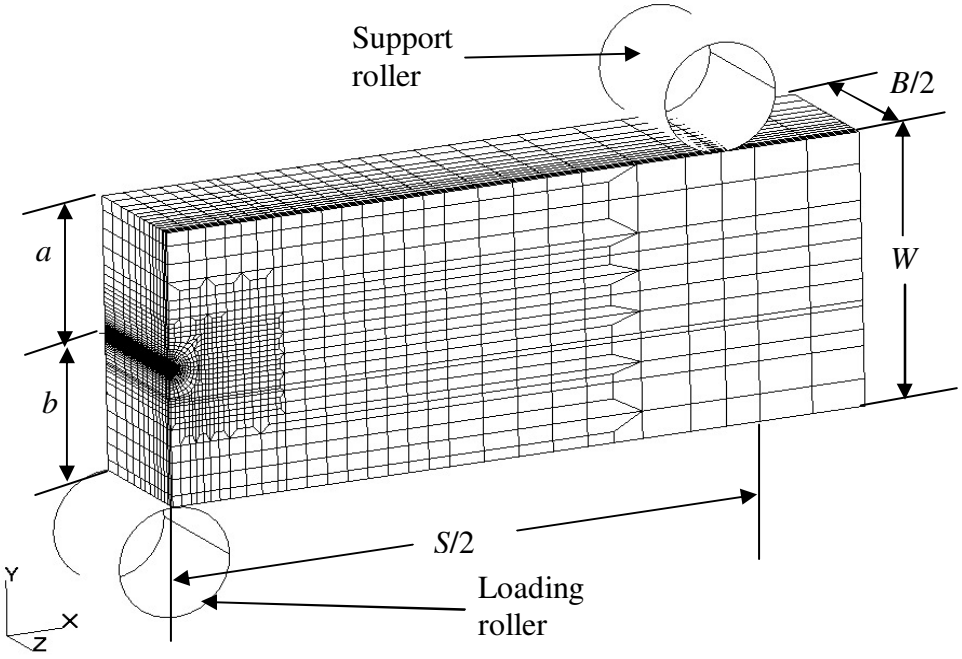

Figure 1. Quarter-symmetric finite element model for a plane-sided SE(B) specimen

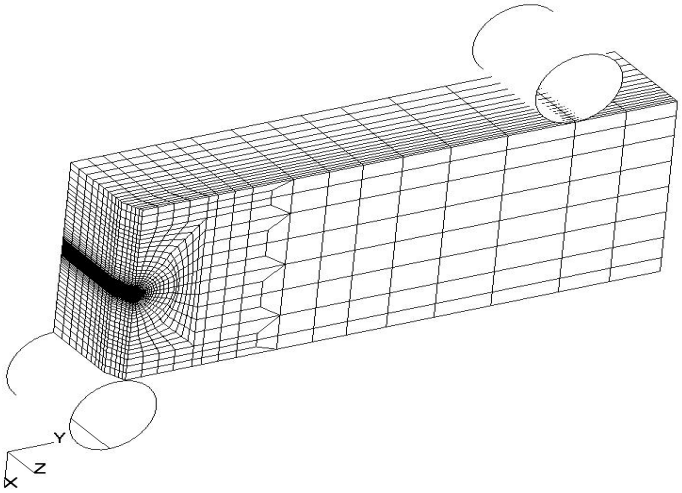

Figure 2. Quarter-symmetric finite element model for a side-grooved SE(B) specimen

$$u(R,\theta)=K\frac{1+\upsilon}{E}\sqrt{\frac{R}{2\pi}}\cos(\frac{1}{2}\theta)(3-4\upsilon-\cos\theta) \tag{7}$$

$$v(R,\theta)=K\frac{1+\upsilon}{E}\sqrt{\frac{R}{2\pi}}\sin(\frac{1}{2}\theta)(3-4\upsilon-\cos\theta) \tag{8}$$

The SSY model used for analysis (see figure 3) has one layer of 2,770 three-dimensional elements with plane-strain constraints (i.e., w = 0 imposed at all nodes). Under plane strain, small-scale yielding (SSY) condition: $J=K^2(1-\upsilon^2)/E$.

The constant ς in Equation (3) can be calculated for a given m and the applied J value obtained from ABAQUS.

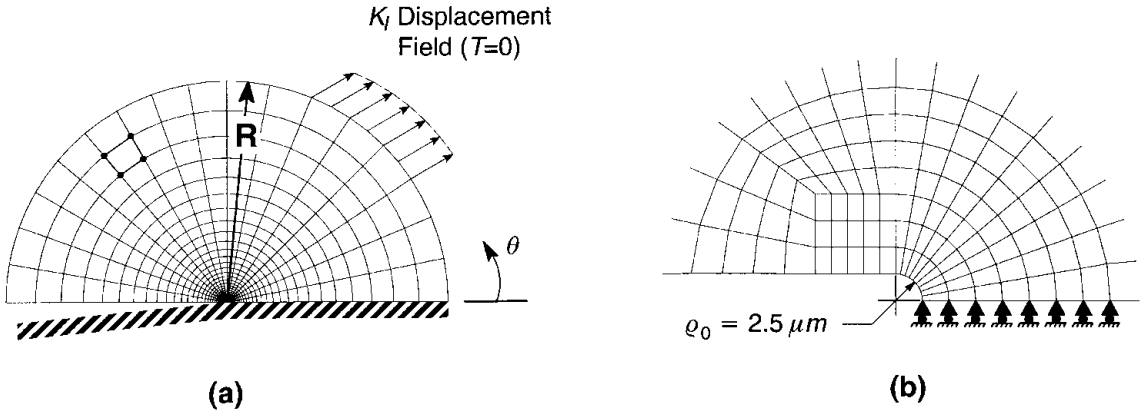

Figure 3. **(a) The small-scale yielding (SSY) model.**
(b) Near-tip mesh, where the initial root radius is 2.5 μm

3.5 Numerical computation of the Weibull stress

In this section, we summarize the finite element form of the Weibull stress, defined by Equation (2).

$$\sigma_w=\left[\frac{1}{V_0}\sum_{n_e}\int_{-1}^{1}\int_{-1}^{1}\int_{-1}^{1}\sigma_1^m\,|J|\,d\eta_1\,d\eta_2\,d\eta_3\right]^{1/m} \tag{9}$$

where n_e is the number of elements inside the fracture process zone. The process zone includes all elements within the crack tip plastic zone. A post-processing program is developed in FORTRAN to compute the Weibull stress using the finite element results of ABAQUS. For all calculations the reference volume (V_0) is taken to be 1 mm^3 for purpose of convenience.

4. NUMERICAL RESULTS

In this section we describe the results obtained from the detailed three-dimensional finite element analyses of single edge notch bend (SE (B)) specimens. The through-thickness average value of J quantifies the level of applied loading. The non-dimensional parameter $M = b\sigma_0 / J_{avg}$ defines the loading level scaled to size of the specimen.

The non-dimensional constraint function ($g(M)$) depends on both the material flow properties and the Weibull modulus, but not on absolute size of the specimen. Larger values of $g(M)$ indicate a higher level of constraint at the crack front. For the plane strain, SSY configuration ($T = 0$), $g(M) = 1.0$ regardless of properties of the chosen material. For the fracture specimens, $g(M)$ decreases as the deformation progresses as a result of loss in constraint and the deformation level (M) at which $g(M)$ falls below unity depends on both material flow properties and the Weibull modulus.

In this study, we consider only one set of material flow properties, $n = 10$ having a strength of $E/\sigma_0 = 500$. The effects of scatter in fracture toughness due to variations of micro-crack size distribution enter into the simulations by varying the Weibull modulus with $m = 8$, 12, 16 and 20.

4.1 Effect of different crack-length on the constraint loss *g(M)* for square cross-section, plane-sided SE(B)

Plane-sided SE(B) specimen with (i) $a/W = 0.5$, $W = B$ and $S = 4W$, and (ii) $a/W = 0.1$, $W = B$ and $S = 4W$, for $n = 10$, $E/\sigma_0 = 500$ and $\upsilon = 0.3$ material constants are considered. In Figure 4 and Figure 5 is shown the computed g-function for a given material property. The g-function describes the evolution of constraint loss over the loading history relative to the plane-strain small-scale yielding (SSY) reference condition (i.e.: zero T-stress). At low load levels ($M > 200$), portions of the g-function curves generally lie above 1.0 for large values of m. This behavior is essentially due to the positive T-stress inherent in deep-notch SE (B) geometry. The smaller m values cause $g(M)$ to drop below 1.0 even at low load levels since they tend to increase the relative contribution to σ_w from the material that is lower stressed and situated at a greater distance from the crack-front and both at and near the free surface.

The shallow cracked specimens show low levels of constraint. Further, the constraint curves for the different Weibull modulus (m) are close indicating a smaller effect of the parameter (m).

4.2 Effect of different crack-length on constraint loss *g(M)* for rectangular cross-section, plane-sided SE(B)

Considering a plane-sided SE (B) specimen for (i) $a/W = 0.5$, $W = 2B$ and $S = 4W$, and (ii) $a/W = 0.1$, $W = 2B$ and $S = 4W$, for the material having $n = 10$, $E/\sigma_0 = 500$ and $\upsilon = 0.3$, in Figure 6 and Figure 7 is shown the g-function. For the case of the deep-notch specimen, the loss in constraint increases once the deformation level goes beyond

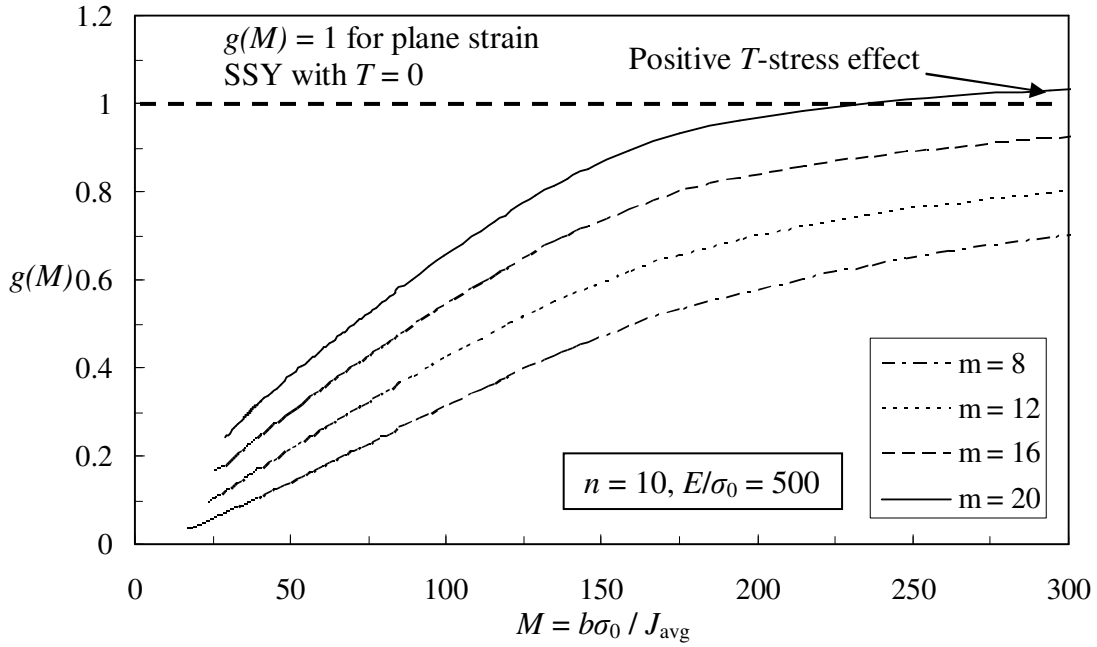

Figure 4. **The non-dimensional constraint function, *g(M)*, for the plane-sided square cross-section SE(B) specimen with *a/W* =0.5.**

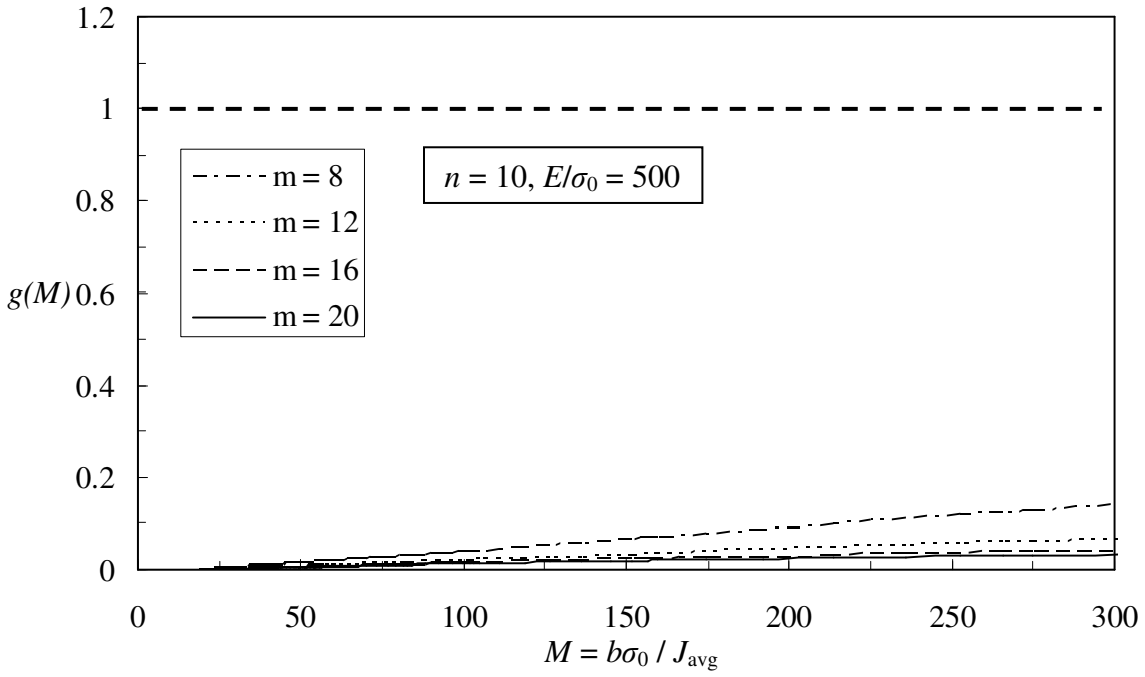

Figure 5. **The non-dimensional constraint function, *g(M)*, for the plane sided square cross-section SE(B) specimens with *a/W* =0.1.**

$M < 150$. The smaller values of m show a lower level of constraint since they tend to increase the relative contribution to Weibull stress from the material that is lower stressed. However, for the specimen having a shallow-notch, the constraint levels are low, which is quite similar to the behavior of a square cross-section.

Table 1. Non-dimensional constraint function *g(M)* for plane-sided specimens

		Square cross-section plane-sided specimen		Rectangular cross-section plane-sided specimen	
m	***M***	**Deep crack specimen *g(M)***	**Shallow crack specimen *g(M)***	**Deep crack specimen *g(M)***	**Shallow crack specimen *g(M)***
20	300	1.05	0.02	0.92	0.03
	150	0.9	0.02	0.73	0.01
	50	0.35	0	0.42	0.005
16	300	0.9	0.03	0.76	0.06
	150	0.73	0.02	0.6	0.02
	50	0.3	0	0.3	0.005
12	300	0.72	0.04	0.6	0.08
	150	0.55	0.02	0.35	0.05
	50	0.18	0	0.15	0.005
8	300	0.63	0.12	0.53	0.15
	150	0.49	0.05	0.33	0.06
	50	0.13	0.01	0.1	0.005

4.3 Effect of side-groove on constraint loss g(M) for a square cross-section, side-grooved SE (B)

Consider a side-grooved SE(B) specimen for (i) $a/W = 0.5$, $W = B$ and $S = 4W$, and (ii) $a/W = 0.1$, $W = B$ and $S = 4W$ for a material having $n = 10$, $E/\sigma_0 = 500$ and $\upsilon = 0.3$, in Figure 8 and Figure 9 is shown the computed g-function. For the deep-notch specimen higher values of the Weibull modulus (m) we see only a positive T-stress.

4.4 Effect of side-groove on the constraint loss g(M) for rectangular cross-section, side-grooved SE (B)

Here we consider a side-grooved SE(B) specimen with (i) $a/W = 0.5$, $W = 2B$ and $S = 4W$, and (ii) $a/W = 0.1$, $W = 2B$ and $S = 4W$, for a material with $n = 10$, $E/\sigma_0 = 500$ and $\upsilon = 0.3$. The computed g-function is shown in Figure 10 and Figure 11. We observe the loss in constraint to be less when compared to the deep-notched specimens, which shows a severe loss in constraint for deformation scale $M < 150$.

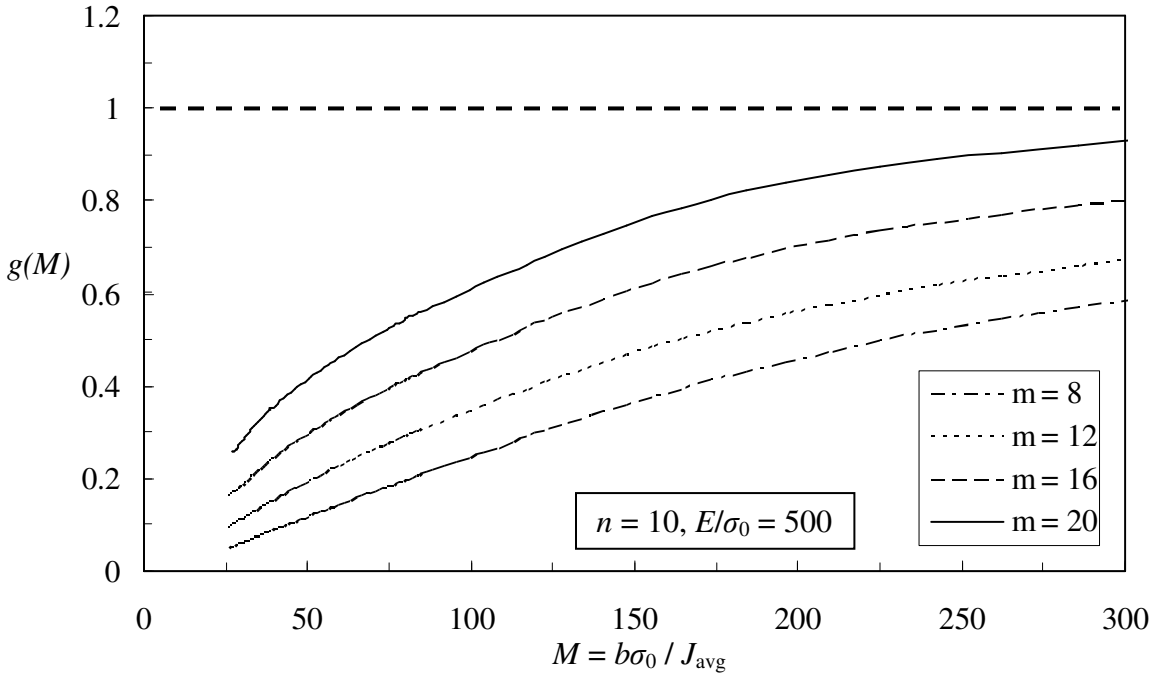

Figure 6. **The non-dimensional constraint function, *g(M)*, for the plane-sided rectangular cross-section SE(B) specimens with *a/W* = 0.5.**

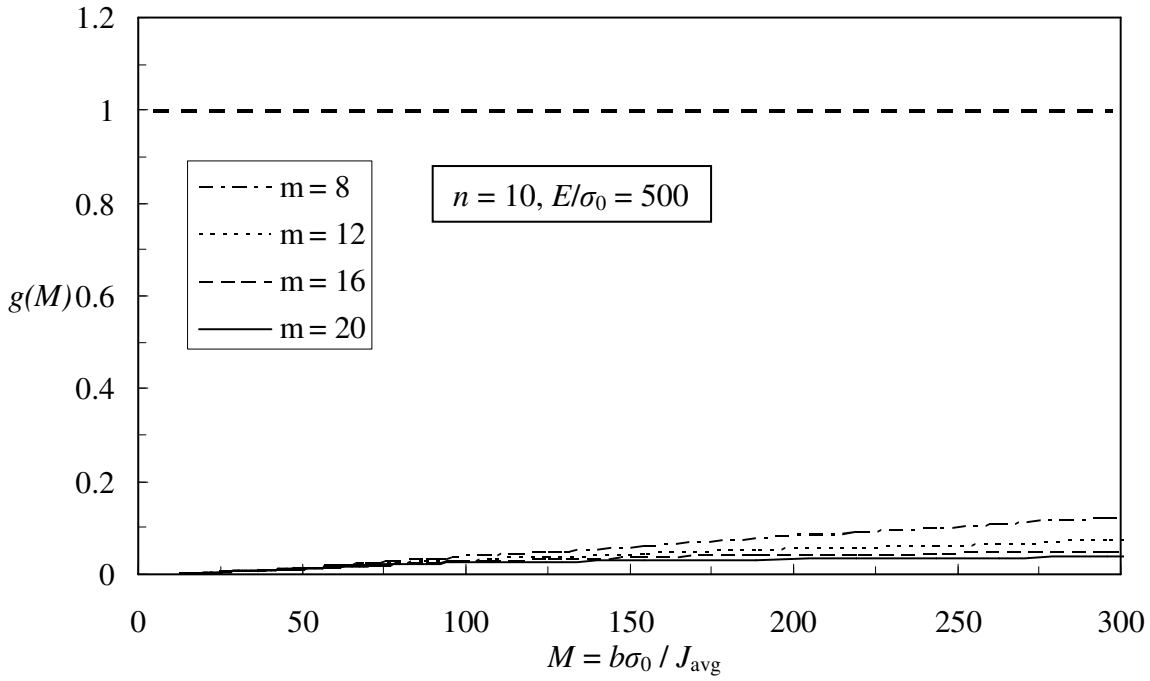

Figure 7. **The non-dimensional constraint function, *g(M)*, for the plane-sided rectangular cross-section SE(B) specimens for *a/W* = 0.1.**

5. CONCLUSIONS

Based on this detailed numerical study the following are the key findings:

1. The non-dimensional *g*-function, defines the evolution of constraint.
   Larger values of *g (M)* imply higher levels of constraint; *g (M)* = 1.0 for plane strain, small scale yielding (SSY) (with *T*-stress = 0), while for the SE (B) specimens, the value of *g (M)* decreases as deformation level increases.

2. The *a*/*W* ratio greatly affects the Weibull stress (σ_w) and hence the constraint function *g (M)*. As a result, shallow cracked specimens have low Weibull stress compared to the deep cracked specimens for the same *J*-level.
   Crack-tip plastic zone in single edge notched bend specimen (SE (B)) having a shallow crack combines with the global bending plasticity very early in the loading.
   A large loss of crack-tip constraint follows and this would require larger *J*-values to generate sufficient stresses and trigger cleavage.

3. The square cross-section (W/B =1) specimen shows slightly more constraint than the rectangular cross-section specimen (W/B = 2).

4. Presence of side grooves raises the constraint level in the SE(B) specimens.

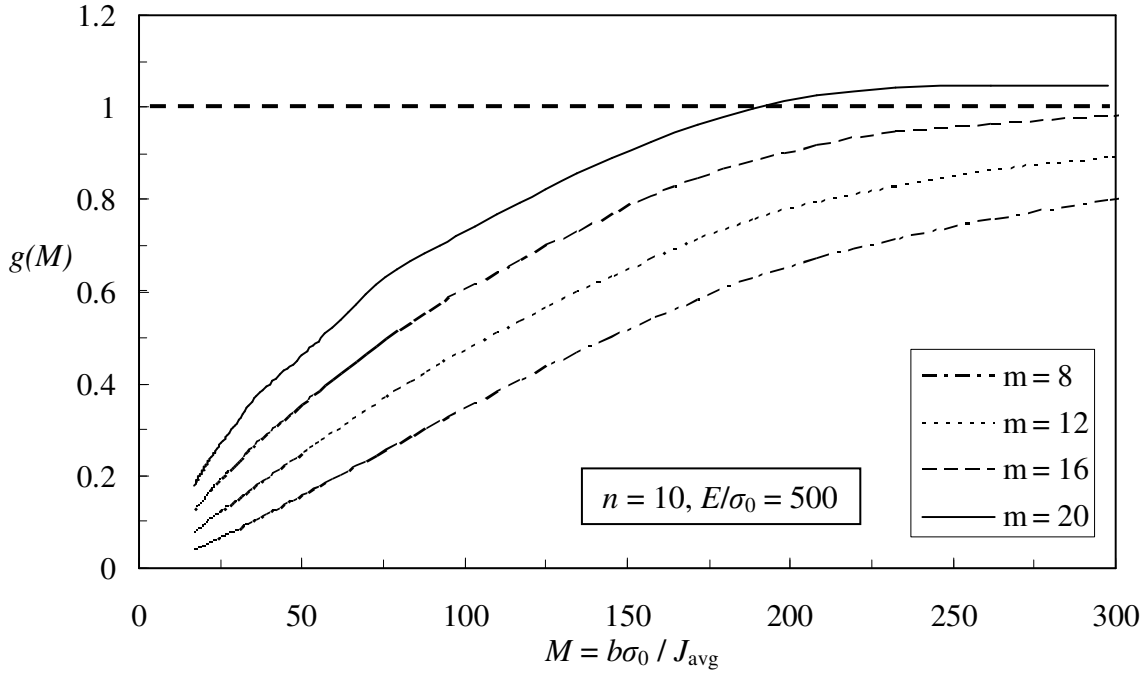

Figure 8. The non-dimensional constraint function, *g(M)*, for the side-grooved square cross-section SE(B) specimens for *a*/*W* = 0.5.

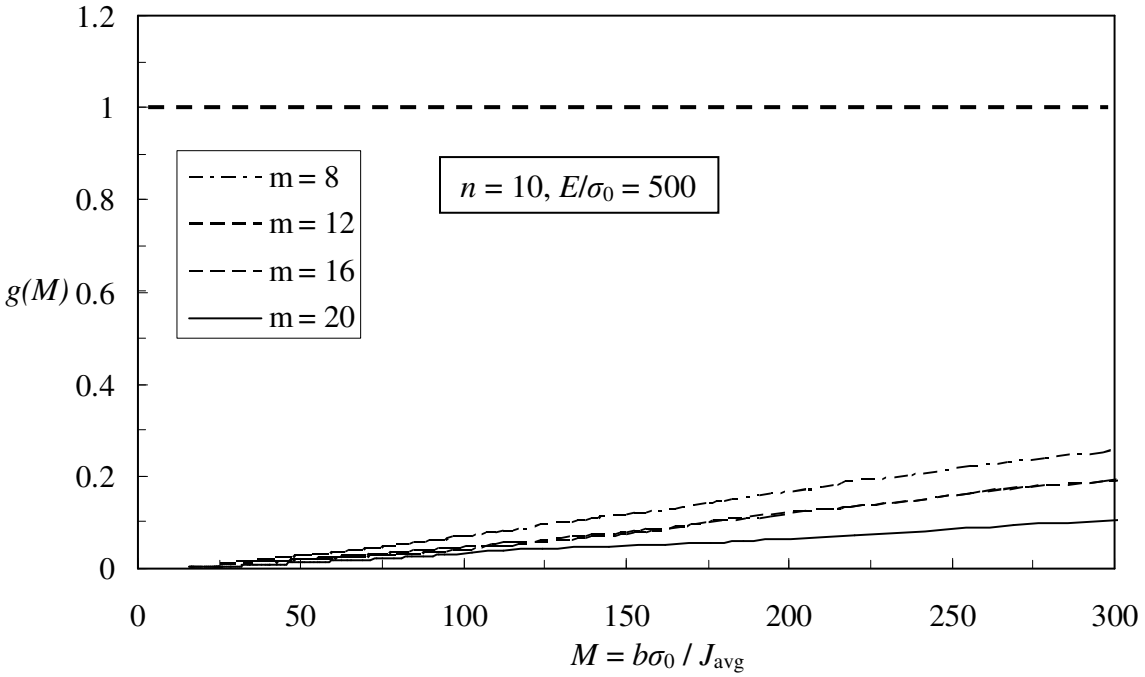

Figure 9. **The non-dimensional constraint function, *g (M)*, for the side-grooved square cross-section SE(B) specimens with *a/W* = 0.1.**

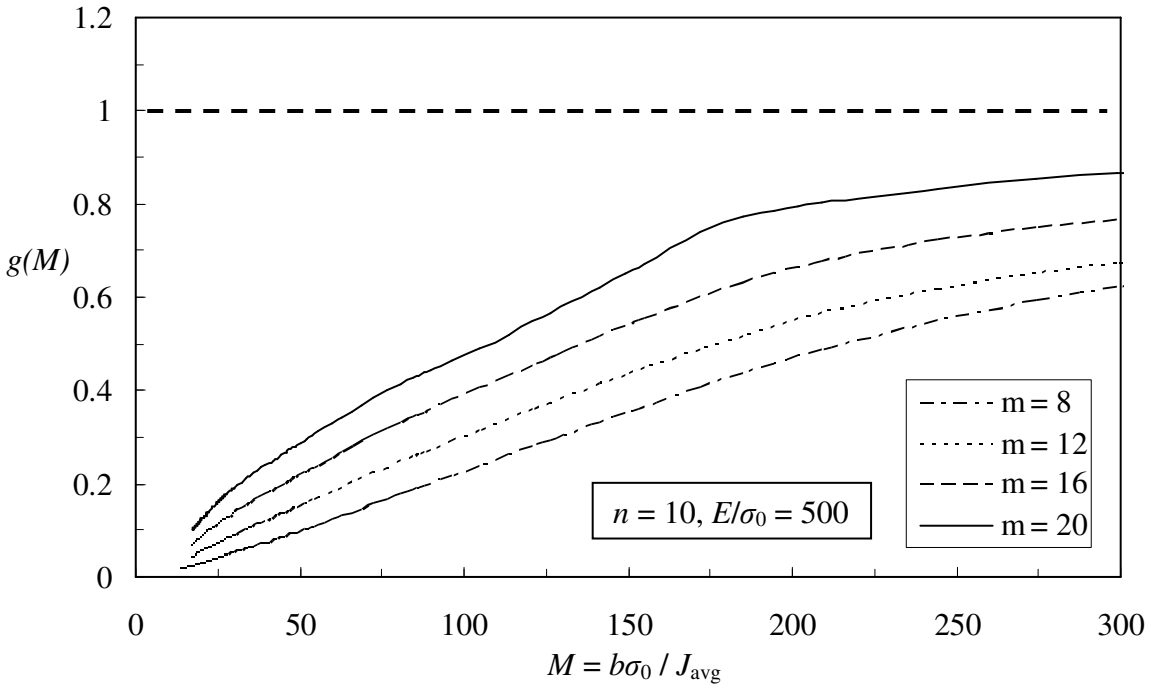

Figure 10. **The non-dimensional constraint function, *g(M)*, for the side-grooved rectangular cross-section SE(B) specimens with *a/W* =0.5.**

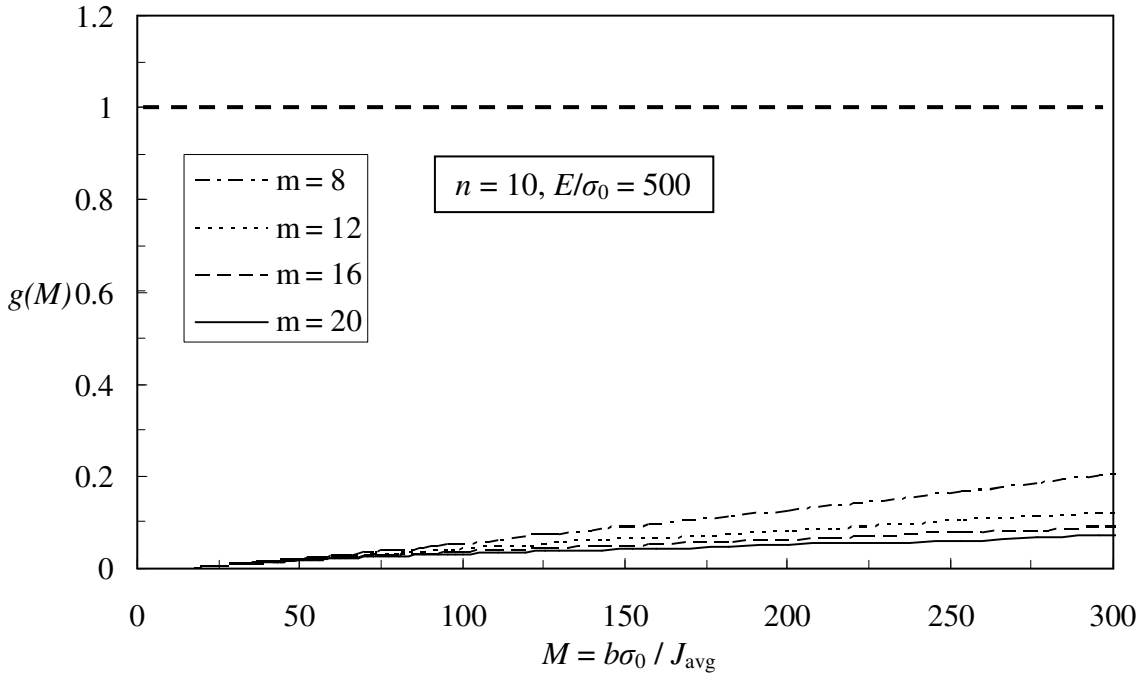

Figure 11. **The non-dimensional constraint function, *g(M)*, for the side-grooved rectangular cross-section SE(B) specimens with *a*/*W* = 0.1.**

Table 2. Non-dimensional constraint function *g(M)* for side-grooved specimens

		Square cross-section side-grooved specimen		Rectangular cross-section side-grooved specimen	
m	***M***	**Deep crack specimen *g(M)***	**Shallow crack specimen *g(M)***	**Deep crack specimen *g(M)***	**Shallow crack specimen *g(M)***
20	300	1.03	0.08	0.83	0.08
	150	0.9	0.05	0.64	0.05
	50	0.47	0.005	0.31	0.005
16	300	0.98	0.18	0.72	0.07
	150	0.76	0.05	0.5	0.05
	50	0.33	0.005	0.19	0.005
12	300	0.85	0.18	0.61	0.09
	150	0.58	0.05	0.42	0.06
	50	0.24	0.01	0.15	0.005
8	300	0.78	0.22	0.57	0.2
	150	0.47	0.12	0.31	0.09
	50	0.13	0.05	0.08	0.01

REFERENCES

[1] American Society for Testing and Materials, Philadelphia. (1998) Test Method for the Determination of Reference Temperature T_0 for Ferritic Steels in the Transition Range (ASTM E 1921).

[2] ABAQUS, V6.7 (2007) ABAQUS reference manuals. 2007. Providence, RI.

[3] Beremin, F.M. (1983) A local criterion for cleavage fracture of a nuclear pressure vessel steel. *Metallurgical Transactions*. 14A, 2277-2287.

[4] Gao, X, Ruggieri and Dodds, R.H. (1998) Calibration of Weibull stress parameters using fracture toughness data. *International Journal of Fracture.* 92,175-200.

[5] Gao, X and Dodds, R.H. (2000) Constraint effects on the ductile-to-brittle transitiontemperature of ferritic steels, a Weibull stress model. *International Journal of Fracture*. 102, 43-69.

[6] Larsson, S.G and Carlsson, A.J. (1973) Influence of non-singular stress terms and specimen geometry on small scale yielding at crack-tips in elastic-plastic materials. *Journal of Mechanics and Physics of Solids*. 21, 263-277.

[7] Mudry, F. (1987) A local approach to cleavage fracture. *Nuclear Engineering and Design*. 105, 65-76.

[8] Minami, F, Bruckner-Foit, A, Munz, D and Trolldenier, B. (1992) Estimation procedure for the Weibull parameters used in the local approach. *International Journal of Fracture*. 54, 197-210.

[9] MSC/PATRAN (2005) MSC Software Inc.

[10] Prakash, S, Gao, X and Srivatsan, T.S. (2009) Numerical modeling of constraint effects on cleavage fracture toughness, Neural, Parallel and Scientific Computations, 17, 445-462.

[11] Rice, J.R. (1968) A path-independent integral and the approximation analysis of strain concentration by notches and cracks, *Journal of Applied Mechanics*, *Transactions ASME*, 35, 379-386.

[12] Rice, J.R. (1974) Limitations to the small scale yielding approximation for crack tip plasticity. *Journal of Mechanics and Physics of Solids*. 22, 17-26.

[13] Sorem, W.A, Dodds, R.H and Rolfe, S.T. (1991) Effects of crack depth on elastic-plastic fracture toughness. *International Journal of Fracture*, 47, 105-126.

[14] Wallin, K. (1984) The scatter in K_{IC} results, *Engineering Fracture Mechanics*, 19, 1085-1093.

[15] Williams, M.L. (1957) On the stress distribution at the base of a stationary crack. *Journal of Applied Mechanics*. 24, 109-114.